
QUANTIFYING DEGENERACY IN SINGULAR MODELS VIA THE LEARNING COEFFICIENT

Edmund Lau

School of Mathematics and Statistics
University of Melbourne
elau1@student.unimelb.edu.au

Daniel Murfet

School of Mathematics and Statistics
University of Melbourne
d.murfet@unimelb.edu.au

Susan Wei

School of Mathematics and Statistics
University of Melbourne
susan.wei@unimelb.edu.au

ABSTRACT

Deep neural networks (DNN) are singular statistical models which exhibit complex degeneracies. In this work, we illustrate how a quantity known as the *learning coefficient* introduced in singular learning theory quantifies precisely the degree of degeneracy in deep neural networks. Importantly, we will demonstrate that degeneracy in DNN cannot be accounted for by simply counting the number of “flat” directions. We propose a computationally scalable approximation of a localized version of the learning coefficient using stochastic gradient Langevin dynamics. To validate our approach, we demonstrate its accuracy in low-dimensional models with known theoretical values. Importantly, the local learning coefficient can correctly recover the ordering of degeneracy between various parameter regions of interest. An experiment on MNIST shows the local learning coefficient can reveal the inductive bias of stochastic optimizers for more or less degenerate critical points.

1 Introduction

Most models in machine learning are **singular**: there are points in parameter space where small changes to the parameter leave the model unchanged (Watanabe, 2007). While these degenerate parameters form a measure zero subset, their effect is far from negligible. In particular, Singular Learning Theory (SLT) shows that the geometry of these degenerate points determines the asymptotics of learning (Watanabe, 2009). The theory explains observable effects of degeneracy in common machine learning models under practical settings (Watanabe, 2018) and has the potential to account for important phenomena in deep learning (Wei et al., 2022) such as phase transitions.

The two central quantities of SLT are the **learning coefficient** λ and **singular fluctuation** ν . Many notable SLT results are conveyed through them. They correspond roughly to the complexity and functional diversity of the model class. Their theoretical values have been documented in only a limited number of settings (Aoyagi and Watanabe, 2005, 2006).

In this work, we are interested in the **local learning coefficient** $\lambda(w^*)$ and **local singular fluctuation** $\nu(w^*)$ for some parameter of interest w^* . Our first contribution is to lay out theoretical conditions that render these local quantities well-defined. Our second contribution is to explain why the local learning coefficient captures the true nature of degeneracy in singular models in a way that Hessian-based measures simply cannot, for the existence of zero eigenvalues of the Hessian in DNNs is more than a technical annoyance. Rather, a complete shift in perspective is required for singular models and SLT provides exactly the tools to do so.

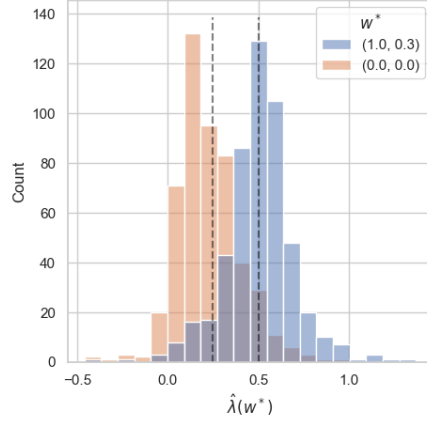


Figure 1: Distribution of $\hat{\lambda}(w^*)$ for two different critical points w^* ; the vertical lines indicate the true $\lambda(w^*)$ with smaller indicating more degenerate. Note the estimates, on average, respect the true ordering of $\lambda(w^*)$. See Section 10.2 for details.

Our final major contribution is to propose a scalable estimator $\hat{\lambda}(w^*)$ that accurately reflects the level of degeneracy around w^* . Our focus is on getting the *ordinality* correct. We establish experimentally that, on average, $\hat{\lambda}(w_A^*) < \hat{\lambda}(w_B^*)$ exactly when $\lambda(w_A^*) < \lambda(w_B^*)$, that is, when w_A^* is more degenerate than w_B^* :

- In a theoretical setting where we know the true $\lambda(w^*)$, our estimator $\hat{\lambda}(w^*)$ recovers the correct ordinality between w^* with different degeneracy (Figure 1).
- In a feedforward ReLU network with $1.9m$ parameters trained on MNIST, we show that $\hat{\lambda}(w^*)$ is smaller when w^* is optimised by entropy-SGD (an optimiser which actively seeks more degenerate parameters) compared to SGD (Figure 2).

Despite the negative connotation of the word “degeneracy”, we emphasise that degeneracy should not be viewed as a deficient quality of singular models. Rather, we conjecture that the nature of the degeneracy of DNNs might be the secret sauce behind their state-of-the-art performance on a wide range of tasks. Our proposed measure of degeneracy could pave the way for a better understanding of the implicit biases induced by the optimisation scheme, the data, etc.

In this paper although we focus mostly on $\hat{\lambda}(w^*)$ as a measure of degeneracy, we also detail the estimator $\hat{\nu}^{\beta^*}(w^*)$ for the sake of completeness and discuss its experimental results. The main application of the local singular fluctuation is in connection with phase transitions and will be treated in future work.

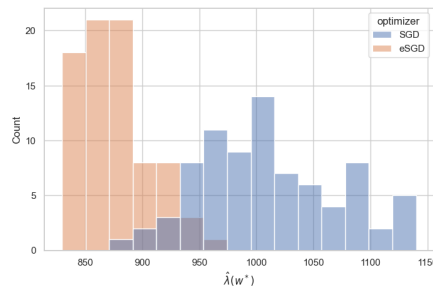


Figure 2: Distribution of $\hat{\lambda}(w^*)$ for minima found by SGD and entropy-SGD in feedforward ReLU network for MNIST. As expected $\hat{\lambda}(w^*)$ for entropy-SGD is lower than for SGD since the former actively seeks out more degenerate critical points. See Section 10.3 for details.

2 Learning coefficient and singular fluctuation

In this section we define the (global) learning coefficient λ and (global) singular fluctuation ν . Let $W \subset \mathbb{R}^d$ be the compact space of parameters $w \in W$. Consider the model-truth-prior triplet

$$(p(x, y|w), q(x, y), \varphi(w)), \quad (1)$$

where $q(x, y) = q(y|x)q(x)$ is the true data-generating mechanism, $p(x, y|w) = p(y|x, w)q(x)$ is the posited model with parameter w , and φ is a prior on w . We assume the triplet satisfies the so-called fundamental conditions in SLT (Watanabe, 2009).

Definition 1. A statistical model $p(x, y|w)$ is called **regular** if it is identifiable, i.e. the parameter to distribution map $w \mapsto p(-|w)$ is one-to-one, and its Fisher information matrix $I(w)$ is everywhere positive definite. We call a model **singular** if it is not regular.

Let $K(w)$ be the Kullback-Leibler divergence

$$K(w) := \text{KL}(q(y|x) \| p(y|x, w))$$

and set

$$K_0 = \inf_{w \in W} K(w).$$

The **truth is realisable by the model** if there exists $w_0 \in W$ such that $q(x, y) = p(y|x, w_0)q(x)$, or equivalently $K_0 = 0$. We do not assume that our models are regular or that the truth is realisable, but we assume the model-truth-prior triplet satisfies the more general condition of **relative finite variance** (Watanabe, 2013). We also assume that there exists w_0^* in the interior of W satisfying $K(w_0^*) = K_0$.

Definition 2. The **zeta function** of the statistical learning system (1) is $\zeta(z) = \int_W (K(w) - K_0)^z \varphi(w) dw$. Let $-\lambda \in \mathbb{R}$ be the largest pole of ζ and m its multiplicity. Then, the **learning coefficient** and its **multiplicity** are given by λ and m respectively.

Let

$$W_0 := \{w \in W : K(w) = K_0\}$$

be the **set of optimal parameters**. When $p(y|x, w)$ is a singular model, W_0 is an analytic variety which is in general positive dimensional (not a collection of isolated points). As long as $\varphi > 0$ on W_0 the learning coefficient λ is equal to a birational invariant of W_0 known in algebraic geometry as the **Real Log Canonical Threshold (RLCT)**. We will always assume this is the case, and now recall how λ is described geometrically.

With $W_\epsilon = \{w \in W : K(w) - K_0 \leq \epsilon\}$ for sufficiently small ϵ , resolution of singularities (Hironaka, 1964) gives us the existence of a birational proper map $g : M \rightarrow W_\epsilon$ which *monomializes* $K(w) - K_0$ in the following sense, described precisely in (Watanabe, 2009, Theorem 6.5): there are local coordinate charts M_α covering $g^{-1}(W_0)$ with coordinates u such that the reparameterisation $w = g(u)$ puts $K(w) - K_0$ and $\varphi(w)dw$ into *normal crossing form*

$$K(g(u)) - K_0 = u_1^{2k_1} \dots u_d^{2k_d} \quad (2)$$

$$|g'(u)| = b(u)u_1^{h_1} \dots u_d^{h_d} \quad (3)$$

$$\varphi(w)dw = \varphi(g(u))|g'(u)|du \quad (4)$$

for some positive smooth function $b(u)$. The (global) RLCT of $K(w) - K_0$ is independent of the (non-unique) resolution map g , but may be computed as (Watanabe, 2009, Definition 6.4)

$$\lambda = \min_{\alpha} \min_{j=1 \dots d} \frac{h_j + 1}{2k_j}. \quad (5)$$

For $P \in W_0$ there exist coordinate charts M_{α^*} such that $g(0) = P$ and (2), (3) hold. The **local RLCT** of $K(w) - K_0$ at P is then (Watanabe, 2009, Definition 2.7)

$$\lambda(P) = \min_{\alpha^*} \min_{j=1 \dots d} \frac{h_j + 1}{2k_j}. \quad (6)$$

The global RLCT λ is the infimum over W_0 of all the local RLCTs $\lambda(P)$. In regular models, all local RLCTs are $d/2$ and hence the global $\lambda = d/2$ and $m = 1$, see (Watanabe, 2009, Remark 1.15).

Next we introduce the singular fluctuation ν^β using a characterisation that is particularly accessible and relates well to our local estimator later in Section 8. See (Watanabe, 2009, Ch. 5, 6) for alternative characterisations of ν^β . Given

an i.i.d. dataset $\mathcal{D}_n = \{(x_i, y_i)\}_{i=1\dots n}$ of size n generated from the true distribution $q(x, y)$, the **functional variance** is defined as

$$V_n^\beta := \sum_{i=1}^n \{E_w^\beta[\log p(y_i|x_i, w)^2] - (E_w^\beta[\log p(y_i|x_i, w)])^2\} \quad (7)$$

where

$$E_w^\beta[f(w)] := \int f(w)p^\beta(w|\mathcal{D}_n) dw$$

denotes expectation of $f(w)$ with respect to $p^\beta(w|\mathcal{D}_n)$, the tempered posterior distribution at inverse temperature β introduced later in (10).

Let $E_{\mathcal{D}_n}$ denote the expectation over the training datasets \mathcal{D}_n . By (Watanabe, 2009, Theorem 6.10), the expected functional variance converges to a constant:

$$\lim_{n \rightarrow \infty} E_{\mathcal{D}_n}[V_n^\beta] = \frac{2}{\beta} \nu^\beta \quad (8)$$

Here ν^β is known as the **singular fluctuation**. Note that ν depends on β though we often suppress the dependency for succinctness.

We have defined the learning coefficient λ and singular fluctuation ν^β for a model-truth-prior triplet (p, q, φ) . Conditions under which their local counterparts, $\lambda(w^*)$ and $\nu(w^*)$, are well-defined quantities are laid out in Section 6. In the meantime we build up to these local quantities by explaining their genesis from the free energy and local free energy formulas.

3 Free energy

In order to recapitulate the role of the learning coefficient as a measure of model complexity, we begin by reviewing the relationship between the free energy and the Bayesian information criterion for model selection. This will set the stage for comparing *regions* of parameter space which is itself a form of model selection governed by the *local* free energy, introduced in Section 6.

To begin, let L_n be the empirical negative log likelihood function

$$L_n(w) = -\frac{1}{n} \sum_i \log p(y_i|x_i, w). \quad (9)$$

The posterior distribution at inverse temperature β is

$$p^\beta(w|\mathcal{D}_n) = \frac{1}{Z_n^\beta} \exp\{-n\beta L_n(w)\} \varphi(w), \quad (10)$$

where

$$Z_n^\beta = \int \exp\{-n\beta L_n(w)\} \varphi(w) dw$$

is the normalising constant. We drop the superscript β in Z_n^β to denote the normalising constant at inverse temperature $\beta = 1$. The quantity Z_n is also known as the *model evidence* or *marginal likelihood*. The **free energy** is defined as

$$F_n = -\log Z_n.$$

Historically, the free energy has occupied an important role in model selection. Recall, in regular models, the non-degeneracy assumption allows one to invoke the Laplace approximation for the free energy, see, e.g., Chapter 8 of (Bleistein and Handelsman, 1986).

Theorem 1 (Laplace Approximation). *Let w_0 be a unique zero of $K(w)$ with positive-definite Hessian $H(w_0) = \nabla^2 K(w_0)$ and $\varphi(w)$ be smooth and non-zero at w_0 . The free energy has asymptotic expansion in n given by*

$$F_n = nL_n(w_0) + \frac{d}{2} \log n - \log \varphi(w_0) - \frac{d}{2} \log(2\pi) + \frac{1}{2} \log \det H(w_0) + O_P(1). \quad (11)$$

The asymptotic in (11) is the basis of the Bayesian Information Criterion (BIC) (Schwarz, 1978), which is equal to the first two terms:

$$\text{BIC} = nL_n(w_0) + \frac{d}{2} \log n.$$

Observe that the geometry of $K(w)$ near w_0 shows up as a direct parameter count d in the $O(\log n)$ term in F_n and the curvature in the principle directions of the Hessian H only show up in the $O(1)$ term. The meaning of lower order terms such as those involving curvature of the likelihood has been explored in such works as (Balasubramanian, 1997).

When $p(y|x, w)$ is a singular model, the Laplace approximation is not valid in general. The **correct asymptotic expansion of the free energy for singular models** is one of the major theorems of SLT. Given an optimal parameter $w_0 \in W_0$, we have

$$F_n = nL_n(w_0) + \lambda \log n - (m - 1) \log \log n + O_P(1). \quad (12)$$

See Watanabe (2009, §3) for the full statement and proof. Note that the condition of relative finite variance is used. When $p(y|x, w)$ is regular, $\lambda = d/2$ and $m = 1$ and so (12) recovers the classic Laplace approximation.

Just as the Laplace approximation is behind the BIC, the asymptotic relation in (12) leads to an idealized information criterion,

$$nL_n(w_0) + \lambda \log n,$$

in which the learning coefficient λ plays the role of $\frac{d}{2}$ in the BIC as a measure of model complexity. In singular models it may be that $\lambda \ll d/2$.

In contrast to the dimension d , the learning coefficient λ is not so readily apparent. It is difficult to derive analytically and so we must turn to computational alternatives. Theorem 4 of (Watanabe, 2013) proposes a practically useful information criterion known as the widely applicable Bayesian information criterion (WBIC),

$$\text{WBIC} := E_w^{\beta^*} [nL_n(w)],$$

where

$$\beta^* = 1/\log n.$$

The WBIC is a good estimator of F_n in the sense that the first two main terms of the WBIC are equal to those of F_n in (12):

$$\text{WBIC} = nL_n(w_0) + \lambda \log n + o_P(\log n).$$

Note that WBIC only requires posterior sampling at a single inverse temperature as opposed to other computational methods for approximating the model evidence, for example via thermodynamic integration (Friel and Pettitt, 2008).

4 Bridging regular and singular models via minimally singular models

This section aims to build intuition by providing a bridge between the familiar notion of regular models and general singular models by studying some familiar kinds of degeneracy. As we discussed in Section 3, Laplace approximation is an oft-used tool to characterize asymptotic behaviors for regular models, in which the set of global minima W_0 of $L(w)$ consists of just one non-degenerate critical point.

There is a slightly more general class of non-identifiable models in which the set of global minima W_0 of the expected negative log-likelihood $L(w)$ consists of (possibly multiple) non-degenerate critical points (making W_0 necessarily a discrete set of points and $L(w)$ a Morse function near W_0). In these cases Laplace approximation can be applied individually to each $w^* \in W_0$. This results in a local version of (11)

$$F_n(B_\gamma(w^*)) = nL_n(w^*) + \frac{d}{2} \log n + \frac{1}{2} \log \det H(w^*) + O_P(1),$$

where $B_\gamma(w^*)$ denotes a neighbourhood of w^* with radius $\gamma > 0$, see (16). For w^* with similar likelihood, hence similar $L_n(w^*)$, the next order term that distinguishes their posterior likelihood is related to their local curvature controlled by the Hessian of the log-likelihood $H(w^*)$. One might call this the most benign form of degeneracy in a statistical model.

Another familiar form of degeneracy arises when W_0 is a smooth submanifold of the parameter space but is non-degenerate in directions normal to W_0 : for $w^* \in W_0$, the Hessian of $L(w)$ restricted to the normal space of $W_0 \subset W$ is a non-singular matrix. We term this kind of model **minimally singular**. While we cannot apply the standard Laplace approximation in this setting, we can invoke a similar result in the form of Morse-Bott Lemma (Banyaga and Hurtubise, 2004), adapted here for local minima only:

Theorem 2. *Let $f : W \rightarrow \mathbb{R}$ be a smooth function of the d -manifold W and let $W_0 \subset W$ the set of global minima which we assume to be a smooth submanifold. Assume that f is a Morse-Bott function in a neighbourhood of W_0 , meaning the Hessian $H_p(f)$ for any $p \in W_0$ restricted to the normal space $N_p W_0$ is non-degenerate. Let C be a k -dimensional connected component of W_0 . Then, for any $p \in C$, there exist a smooth chart centred there, $\phi : U \rightarrow \mathbb{R}^k \times \mathbb{R}^{d-k}$ such that,*

- $\phi(U \cap W_0) = \{(x, y) \in \mathbb{R}^k \times \mathbb{R}^{d-k} : y = 0\}$
- $f \circ \phi^{-1}(x, y) = f(W_0) + y_1^2 + y_2^2 + \dots + y_{d'}^2$

where $d' = \text{codim}(C) = d - k$.

Notice that, if $d' = d$, making $k = 0$, we recover the case where W_0 is a discrete set of non-degenerate critical points described above, i.e. f is just a Morse function. Using the local chart afforded by the theorem, for $w^* \in C$ with $\text{codim}(C) = d'$, we have

$$\begin{aligned} & -\log \int_{B_\gamma(w^*)} e^{-nL(w)} \varphi(w) dw \\ &= -\log \int_{B_\gamma(w^*)} e^{-nL(w^*)} e^{-n \sum_{j=1}^{d'} y_j^2} \phi(x, y) dy dx \\ &= nL(w^*) + \frac{d'}{2} \log n + O(1) \end{aligned}$$

where $\phi(x, y) > 0$ is some positive smooth function and we have invoked the usual Laplace approximation on the inner y -integral. By Jensen's inequality, this gives us an upper bound on the expected local free energy $E_{\mathcal{D}_n} F_n(B_\gamma(w^*))$ which is in fact an asymptotic equality for models satisfying the fundamental conditions of SLT (Watanabe, 2009, Chapter 6).

This result means that, in minimally singular models, the posterior will preferentially concentrate near neighbourhoods of optimal parameters w^* that have low effective dimension d' . Unlike the previous setting where $d' = d$ everywhere on W_0 , the “energy-entropy competition” for minimally singular models plays out by seeking lower effective dimension first before selecting on the basis of local curvature.

For general singular models, there are no obvious generalisations of the Laplace method and one should instead apply resolution of singularities. Furthermore, the notion of “effective dimension” is no longer really appropriate, since the dimension of the normal bundle is not defined at a point $p \in W_0$ where W_0 is not a submanifold. Instead we need to switch to talking about **degeneracy** and SLT posits that the learning coefficient $\lambda(w^*)$ is the correct measure of model degeneracy near w^* .

One important way such degeneracy could arise is if the model admits **continuous symmetry**. In general, more symmetric solution w^* (e.g. locally admits actions of a high dimensional Lie group) would be preferred by the Bayesian posterior as it would result in w^* belonging to a low codimension, d' , neighbourhood of solutions and leading to a tighter upper bound of the learning coefficient, $\lambda \leq d'/2$.

5 Comparing degeneracy in an example

To motivate the local free energy in the next section, we examine a toy example in which the behaviour of the posterior in two regions of parameter space is distinguished by their local learning coefficients, to be rigorously defined in Section 6. This will illustrate why $\lambda(w^*)$ is a measure of degeneracy of the region around w^* , and how the degeneracies that arise in singular models can be more complex than just the number of free parameters (flat directions).

In this section it will be helpful to write the posterior distribution in terms of $K_n(w)$, the empirical counterpart to $K(w)$, given by

$$K_n(w) := \frac{1}{n} \sum_{i=1}^n [\log q(y_i | x_i) - \log p(y_i | x_i, w)]. \quad (13)$$

It is easy to see that the posterior distribution in (10) is equivalently given by

$$p(w | \mathcal{D}_n) = \frac{1}{\bar{Z}_n} \exp\{-n\beta K_n(w)\} \varphi(w). \quad (14)$$

Note that the normalising constant \bar{Z}_n in (14) differs from Z_n in (10) by a constant and thus the distinction between the two is immaterial to the subsequent asymptotic analysis.

We make one final simplifying step. For building theoretical intuition, we consider the **stylised posterior**

$$p(w | \mathcal{D}_\infty) \propto \exp\{-nK(w)\} \varphi(w)$$

which depends on n but with the stochasticity in K_n removed and replaced by the deterministic K . Let

$$\bar{Z}_{n,K} = \int \exp\{-nK(w)\} \varphi(w) dw$$

be the normalising constant of the stylised posterior. We will study it in place of \bar{Z}_n which is studied in place of Z_n .

Our toy example is a model with parameter space $W \subseteq \mathbb{R}^2$ and chosen so that the KL divergence is

$$K(w_1, w_2) = (w_1 - 1)^2 (w_1^2 + w_2^2)^4. \quad (15)$$

The optimal parameter set has two components: $W_0 = U \cup V$ where U is the line $w_1 = 1$ and V the point at the origin. Let U_γ, V_γ be sufficiently small neighbourhoods of U, V respectively. These are the regions we seek to compare, both in terms of the concentration of the Bayesian posterior as $n \rightarrow \infty$ and in terms of degeneracy of the critical points of K they contain.

Define the restricted evidence and free energy of the stylised posterior to be

$$\begin{aligned} \bar{Z}_{n,K}(U_\gamma) &= \int_{U_\gamma} \exp\{-nK(w_1, w_2)\} dw_1 dw_2 \\ \bar{F}_{n,K}(U_\gamma) &= -\log \bar{Z}_{n,K}(U_\gamma), \end{aligned}$$

and similarly for $\bar{Z}_{n,K}(V_\gamma)$ and $\bar{F}_{n,K}(V_\gamma)$. Note that we take a constant prior on W . This contributes constant terms related to the volume of U_γ, V_γ (larger regions can have more probability mass simply because they are larger) which become irrelevant for large enough n . To answer the question “in which of the two regions U_γ, V_γ does the stylised posterior concentrate” is to compare $\bar{Z}_{n,K}(U_\gamma), \bar{Z}_{n,K}(V_\gamma)$ or equivalently the free energies.

Noticing that K is non-degenerate in the w_1 -direction normal to the line U (that is, K has non-vanishing second-order w_1 -partial derivative) we can invoke Laplace approximation to prove that

$$\bar{F}_{n,K}(U_\gamma) = \frac{1}{2} \log n + O(1).$$

Every point in U is a degenerate critical point of K (the Hessian has zero eigenvalues) but this degeneracy is of a mild form of what we referred to as **minimally singular** in Section 4: the function K has a local expression as a sum of squares that is less than full (i.e. the expression uses $d' < d$ coordinates).

We now turn our attention to V . Analysis via Laplace approximation must fail for V : if it were valid then since $\text{codim}(V) = 2$, $\bar{F}_{n,K}(V_\gamma)$ would have to behave like $\log n + O(1)$, suggesting a much lower probability mass near V compared to U . However, contrary to this expectation, Figure 3 shows that the stylised posterior will asymptotically concentrate in a small neighbourhood of V instead of U . Indeed, observe that $K \approx r^8 + \text{const}$ in polar coordinates near the origin, making it a *degenerate* critical point for $K(w)$. The correct asymptotic turns out to be

$$\bar{F}_{n,K}(V_\gamma) = \frac{1}{4} \log n + O(1),$$

which is significantly lower than the behaviour suggested by a naive dimension count.

6 Local quantities

Building on the example from the previous section we define the local free energy as a measure of posterior concentration in a parameter region of interest, and explain how the local learning coefficient helps us to reason about this concentration asymptotically as $n \rightarrow \infty$.

To compare the concentration of the Bayesian posterior near w^* with the concentration near other parameters, we would like to understand the quantity

$$Z_n(B_\gamma(w^*)) = \int_{B_\gamma(w^*)} \exp\{-nL_n(w)\} \varphi(w) dw$$

with $B_\gamma(w^*)$ denoting a neighbourhood of w^* of radius γ for some $\gamma > 0$, and the associated **local free energy**

$$F_n(B_\gamma(w^*)) = -\log Z_n(B_\gamma(w^*)). \quad (16)$$

If we set

$$\begin{aligned} \text{vol}(\gamma, w^*) &= \int_{B_\gamma(w^*)} \varphi(w) dw, \\ \bar{\varphi}(w) &= \frac{1}{\text{vol}(\gamma, w^*)} \varphi(w) \end{aligned}$$

then we can form the **local triplet** $(p, q, \bar{\varphi})$ with parameter space $B_\gamma(w^*)$. Let $L(w)$ be the theoretical counterpart to $L_n(w)$, i.e., $L(w) = -\mathbb{E}_{q(x,y)} \log p(y|x, w)$. Our hypotheses on w^* are as follows:

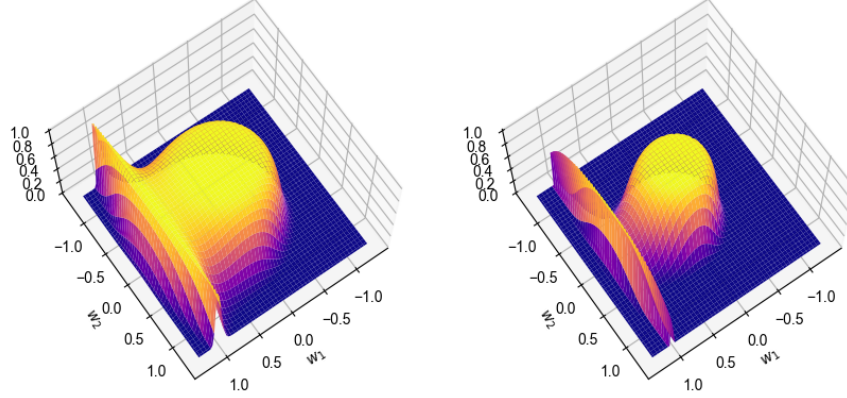


Figure 3: The unnormalized density $\exp\{-nK(w_1, w_2)\}$ for K in (15) visualised at $n = 5$ and $n = 100$. The 0-dimensional component of W_0 (V , learning coefficient $\frac{1}{4}$) dominates the 1-dimensional line (U , learning coefficient $\frac{1}{2}$) in the large n limit due to it being more degenerate.

- $L(w^*) \leq L(P)$ if $P \in B_\gamma(w^*)$.
- $\lambda(w^*) \leq \lambda(P)$ if $P \in B_\gamma(w^*)$ and $L(P) = L(w^*)$.
- The local triplet satisfies relative finite variance.

The first two hypotheses say that w^* is a minimum of L in its neighbourhood and w^* is at least as degenerate as any nearby minimiser. Note that the KL divergence for this triplet is just the restriction of $K : W \rightarrow \mathbb{R}$ to $B_\gamma(w^*)$, but the local triplet has its own set of optimal parameters

$$W_0(w^*, \gamma) = \{w \in B_\gamma(w^*) : L(w) = L(w^*)\}. \quad (17)$$

Applying the definitions of Section 2 and results of Section 3 to the local triplet (replacing W_0 there by $W_0(w^*, \gamma)$), the asymptotic expansion of (12) gives

$$F_n(B_\gamma(w^*)) = nL_n(w^*) + \lambda(w^*) \log n - (m(w^*) - 1) \log \log n + O_P(1), \quad (18)$$

where the difference between $\varphi, \bar{\varphi}$ contributes a summand $\log \text{vol}(\gamma, w^*)$ to the constant term. This explains why we can consider $\lambda(w^*)$ as a **local learning coefficient**, following the ideas sketched in (Watanabe, 2009, Section 7.6).

Recall that the posterior concentration at a given neighbourhood is directly revealed by their local free energy. Equation (18) in turns shows that there is a competition between energy, $nL_n(w^*)$, and entropy, $\lambda(w^*)$. Consequently, in comparing the degeneracy between points w_A^* and w_B^* , it is important to remember that $\lambda(w_A^*) < \lambda(w_B^*)$ is only evidence of greater posterior concentration near w_A^* if the two points are in the same level set of $L(w)$.

7 Estimation of local learning coefficient

The local free energy in (16) is not easy to compute, so we introduce a proxy which we will estimate instead. Specifically, we introduce a localising Gaussian prior that acts as a surrogate for enforcing the domain of integration. Let

$$\varphi_\gamma(w) \propto \exp\left\{-\frac{\gamma}{2} \|w\|_2^2\right\}$$

be a Gaussian prior centred at the origin with scale parameter γ . Define the tempered local posterior centred at $w^* \in W$ with scale γ and inverse temperature β to be

$$p^\beta(w | \mathcal{D}_n, w^*, \gamma) := \frac{\exp\{-n\beta L_n(w)\} \varphi_\gamma(w - w^*)}{Z_n^\beta(w^*, \gamma)} \quad (19)$$

where

$$Z_n^\beta(w^*, \gamma) = \int \exp\{-n\beta L_n(w)\} \varphi_\gamma(w - w^*) dw$$

is the normalising constant. Again we suppress β and write $Z_n(w^*, \gamma)$ when $\beta = 1$. We shall treat

$$F_n(w^*, \gamma) := -\log Z_n(w^*, \gamma)$$

as a proxy for $F_n(B_\gamma(w^*))$. In our estimation procedure, we assume that w^* may be replaced by its empirical estimate

$$\hat{w}_n^* := \arg \min_{w \in B_\gamma(w^*)} L_n(w).$$

Once we have an estimator $\hat{F}_n(w^*, \gamma)$ of $F_n(w^*, \gamma)$, we discard lower order terms in (18) and manipulate to obtain the following estimator of $\lambda(w^*)$:

$$\frac{\hat{F}_n(w^*, \gamma) - nL_n(\hat{w}_n^*)}{\log n}.$$

To estimate $F_n(w^*, \gamma)$ we propose employing a local version of the WBIC leading to the local learning coefficient estimate

$$\hat{\lambda}(w^*) := \frac{\mathbb{E}_{w|\hat{w}_n^*, \gamma}^{\beta^*}[nL_n(w)] - nL_n(\hat{w}_n^*)}{\log n} \quad (20)$$

where

$$\beta^* = \frac{1}{\log n}.$$

Here we have written the expectation of a function $f(w)$ with respect to the tempered local posterior in (19) as

$$\mathbb{E}_{w|w^*, \gamma}^\beta[f(w)] := \int f(w) p^\beta(w|\mathcal{D}_n, w^*, \gamma) dw.$$

Better estimates than (20) are conceivable, e.g., via the techniques set out in Corollary 3 of (Watanabe, 2013), at the cost of doing posterior sampling at multiple inverse temperatures β .

7.1 SGLD-based WBIC

Calculating the local WBIC in (20), $\mathbb{E}_{w|\hat{w}_n^*, \gamma}^{\beta^*}[nL_n(w)]$, requires samples from the posterior in (19) localised at \hat{w}_n^* at inverse temperature $\beta^* = 1/\log n$. The standard WBIC has previously been deployed on small singular models where careful MCMC can be applied (Friel et al., 2017; Imai, 2019). Because our interest is in modern neural networks, we need scalable sampling methods. For this purpose, we chose to employ SGLD (Welling and Teh, 2011) for its simplicity and speed. The SGLD updates for sampling (19) are given by

$$\Delta w_t = \frac{\epsilon}{2} \left(\frac{\beta n}{m} \sum_{i=1}^m \nabla \log p(y_i|x_{l_i}, w_t) + \gamma(w^* - w_t) \right) + N(0, \epsilon)$$

where the log likelihood term is calculated over randomly sampled minibatch of m samples $\{(x_{l_i}, y_{l_i})\}_{i=1}^m$, and ϵ controls the injected Gaussian noise. We use T to denote the total number of SGLD iterations.

8 Estimation of local singular fluctuation

The definition of ν^β in (8) suggests for its estimator,

$$\hat{\nu}^\beta = \frac{\beta}{2} V_n^\beta.$$

Adapting the functional variance estimator for local singular fluctuation estimation is straightforward. In (7), we simply replace \mathbb{E}_w^β with $\mathbb{E}_{w|w^*, \gamma}^\beta$ to arrive at $V_n^{\beta^*}(w^*)$. Let us call the resulting estimate of the local singular fluctuation $\hat{\nu}^{\beta^*}(w^*)$.

Although the case $\beta = 1$ is of particular interest in Bayesian learning (see Appendix A), our local learning coefficient estimates $\hat{\lambda}(w^*)$ are formed by sampling from the tempered local posterior (19) at inverse temperature $\beta^* = 1/\log n$. To avoid additional computation, we calculate the local singular fluctuation estimator $\hat{\nu}^{\beta^*}(w^*)$. Note that it is possible to convert the estimate from one inverse temperature to another inverse temperature via Equation 20 in Watanabe (2013).

9 Related Work

Measuring model complexity is a long-studied problem in statistics and learning theory. Traditional measures such as VC dimension and Rademacher complexity are applied to the entire hypothesis class. Other measures such as the norm-based complexity measure in Liang et al. (2019) and the sensitivity-based complexity measure in Novak et al. (2018) are applied to a specific hypothesis.

Beyond their intrinsic interest, complexity measures also hold the promise of explaining the generalisation puzzle (Zhang et al., 2017) in deep learning. The sheer number of complexity measures proposed towards this end prompted Jiang et al. (2019) to conduct a careful correlation analysis of 40 complexity measures with generalisation. Many of the investigated measures correlate poorly (and even negatively) with generalisation error.

In this work, we are motivated by the correspondence between Bayesian parameter inference and thermodynamics which several recent works have noted (Le, 2018; Zhang et al., 2018; LaMont and Wiggins, 2019). Using the free energy principle, we can understand the extent to which minima with different degrees of degeneracy might be preferred by the Bayesian posterior. A direct inspiration for our work is Zhang et al. (2018) which proposes $\log \det H(w^*)$ as a complexity measure by way of the Laplace approximation in (11). Although correct in spirit, their analysis incorrectly applies the Laplace approximation which does not hold for singular models, and hence neural networks. Indeed, this Hessian-based degeneracy measure is often degenerate with determinant zero. Even after scrubbing the nearly-zero eigenvalues, such a complexity measure cannot capture the type of degeneracy exhibited by singular models, which we illustrated in Section 5. Furthermore, even if the model were minimally singular, the Hessian contribution to the free energy is only $O(1)$.

Finally, we briefly discuss concurrent work that measures a quantity related to the global learning coefficient. In Chen et al. (2023), a measure called the learning capacity is proposed to estimate the complexity of a hypothesis class. The learning capacity can be viewed as a finite- n version of the learning coefficient; the latter only appears in the $n \rightarrow \infty$ limit. Chen et al. (2023) is largely interested in the learning capacity as a function of training size n . They discover the learning capacity saturates at very small and large n with a sharp transition in between.

monomial	λ	MCMC	SGLD	monomial	MCMC	SGLD
$w_1^1 w_2^3$	0.17	0.12 (0.04)	0.11 (0.07)	$w_1^1 w_2^3$	0.17 (0.03)	0.14 (0.05)
$w_1^1 w_2^2$	0.25	0.19 (0.11)	0.14 (0.12)	$w_1^1 w_2^2$	0.32 (0.16)	0.23 (0.09)
$w_1^0 w_2^1$	0.50	0.41 (0.12)	0.45 (0.11)	$w_1^0 w_2^1$	0.50 (0.04)	0.54 (0.04)
$w_1^1 w_2^0$	0.50	0.43 (0.12)	0.47 (0.13)	$w_1^1 w_2^0$	0.49 (0.03)	0.53 (0.05)

(a) Estimates $\hat{\lambda}(w^*)$ (with standard deviation)

(b) Estimates $\hat{\nu}^{\beta^*}(w^*)$ (with standard deviation).

Table 1: Estimates for the normal crossing model-truth-prior triplets described in Section 10.1 using posterior samples from MCMC or SGLD. The hyperparameters in SGLD are set to batch size $m = n$, $\epsilon = 0.0005$ and chain length $T = 10,000$. The estimated local learning coefficients correlate well with their true values.

10 Experiments

In this section we first validate the accuracy of the $\hat{\lambda}(w^*)$ estimator for models that are in normal crossing form. We observe that $\hat{\lambda}(w^*)$ does indeed correlate well with the true $\lambda(w^*)$. Next, we revisit the example in Section 5 to verify that $\hat{\lambda}(w^*)$ can distinguish between parameter regions with different degeneracy.

Finally, we examine a feedforward ReLU network trained on the MNIST dataset. Because we do not know the true critical points corresponding to this model-truth-prior triplet, we shall instead train the network to convergence with two different stochastic optimisers: SGD with momentum and another optimiser designed to minimise a proxy to local free energy known as entropy-SGD Chaudhari et al. (2019). As expected, our local learning coefficient estimator can distinguish the critical points preferred by the two optimisers.

10.1 2D posterior in normal crossing form

Let us study posteriors that are already in normal crossing form as per (2) and (3). The significance and generality of this form is discussed in Section 2. Specifically we consider a regression model with inputs x sampled from a standard

Gaussian and outputs

$$y = \rho(w_1, w_2)x + N(0, \sigma^2)$$

where

$$\rho(w_1, w_2) = w_1^{k_1} w_2^{k_2}$$

is a monomial and $\sigma^2 = 1/4$ is the variance of the observation noise. We fix the prior to be a uniform prior and investigate different $(k_1, k_2) \in \mathbb{N}^2$.

A synthetic training data set of size $n = 1000$ is generated where the true parameter is chosen to be $w^* = (0, 0)$. It can be shown that, with this setup, $K(w) = C w_1^{2k_1} w_2^{2k_2}$ for a positive constant C and $W_0 = \{(w_1, w_2) \in \mathbb{R}^2 : w_1 w_2 = 0\}$. In this simple example, we have theoretical knowledge of the true learning coefficient given by $\lambda = \min\{1/(2k_1), 1/(2k_2)\}$.

Note that in this synthetic setup, there is no need to employ (20) with a plug-in estimate \hat{w}_n^* since we know the true critical point w^* . We compare the effects of different posterior sampling methods, SGLD versus MCMC, on the estimator $\hat{\lambda}(w^*)$. For MCMC, we employ the No U-Turn Sampler Hoffman and Gelman (2014). The scale parameter γ in the localising prior of the SGLD sampler is set to 1.0 and chain length T is set to 10 000.

All experiments are repeated 10 times with different RNG seeds which results in different datasets and different posterior sample paths. Table 1a shows the mean and standard deviation of $\hat{\lambda}(w^*)$ estimates resulting from SGLD and MCMC as well as the theoretical $\lambda(w^*)$. We also display the local singular fluctuation estimates in Table 1b.

Figure 8 shows sample paths taken by SGLD and MCMC for various k_1, k_2 . We see that overall MCMC does indeed explore the posterior better though SGLD is able to explore the most degenerate direction and hence the SGLD-based estimate does not suffer for its limited exploration of the posterior. Regarding the effect of γ on the estimate $\hat{\lambda}(w^*)$, Figure 9 reveals that the estimate can suffer from overly concentrated localising priors.

10.2 2D posterior with neighbourhoods of different degeneracy

Next, we run experiments that numerically illustrate the theoretical results presented in Section 5. Consider the regression model

$$y = \rho(w_1, w_2)x + N(0, \sigma^2)$$

with

$$\rho(w_1, w_2) = (w_1 - 1)(w_1^2 + w_2^2)^2.$$

We generate training data of size $n = 1000$ with noise $\sigma^2 = 1/4$ and the true parameter is set to be at the origin. This leads to $K(w)$ in (15). We choose a uniform prior φ .

To estimate $\hat{\lambda}(w^*)$ for $U = \{(w_1, w_2) \in \mathbb{R}^2 : w_1 = 1\}$ and $V = \{(0, 0)\}$, we respectively set $w_U^* = (1.0, 0.3)$, and $w_V^* = (0.0, 0.0)$ in (20). The scale parameter γ in the localising prior is chosen to be 0.2. The choice of ϵ and chain length T are respectively 0.0001 and 5000. We implement full-batch SGLD for this toy example.

The experiment is repeated 500 times. In Figure 1 we can see that, on average, $\hat{\lambda}(w_V^*) < \hat{\lambda}(w_U^*)$, recovering the theoretically known order of local degeneracy, $\lambda(w_V^*) < \lambda(w_U^*)$. Moreover, both $\hat{\lambda}(w^*)$ distributions concentrate around their true local learning coefficients.

10.3 MNIST

We fit a two hidden-layer feedforward ReLU network with 1.9m parameters to MNIST using two stochastic optimisers: SGD and entropy-SGD (Chaudhari et al., 2019). Our interest in entropy-SGD is due to its objective function being none other than to minimise $F_n(w^*, \gamma)$ over w^* . As such we expect that the local minima found by entropy-SGD will have lower $\hat{\lambda}(w^*)$.

We obtain multiple ($S = 80$) training trajectories resulting in a collection of trained weights $\hat{w}^1, \dots, \hat{w}^S$ for each optimiser. The training data remains fixed in this repetition, only the randomness in the stochastic optimiser is being modded out. We record $\hat{\lambda}(\hat{w}^s), \hat{\nu}^{\beta^*}(w^*)$ for $s = 1, \dots, S$. See Appendix B for complete experimental details. To save on memory and compute, for this MNIST experiment, we actually calculate and report a mini-batch version of $\hat{\lambda}(w^*)$, see details in Appendix C. We have no mini-batch version of $\hat{\nu}^{\beta^*}(w^*)$ implemented at present but it should be tractable.

Figure 2 confirms our expectation that entropy-SGD finds local minima with lower local learning coefficient, i.e., entropy-SGD is attracted to more degenerate critical points than SGD. Figure 2 is simply one of the configurations

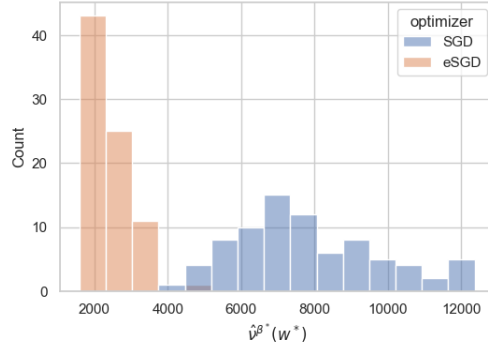


Figure 4: Distribution of $\hat{\nu}^{\beta^*}(w^*)$ for minima found by SGD and entropy-SGD in feedforward ReLU network for MNIST. SGD appears to be more attracted to parameter regions where the local posterior is diverse in function space.

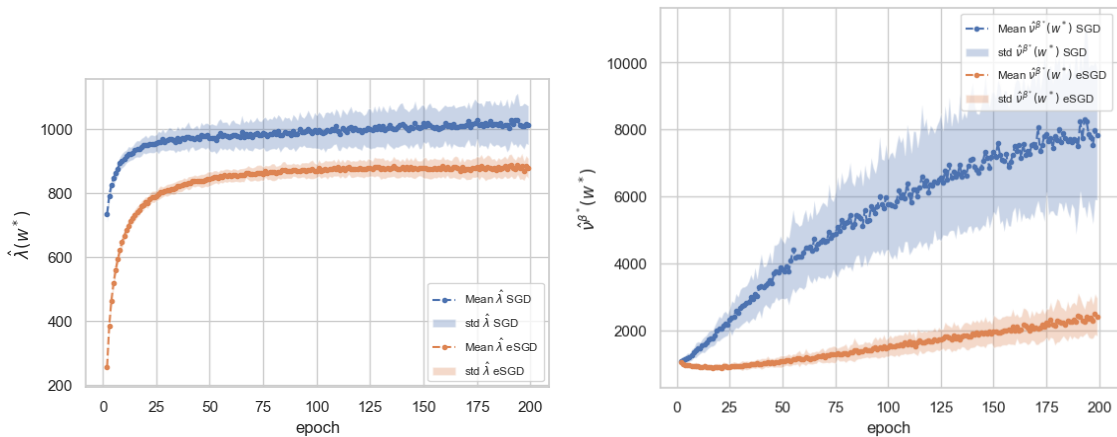


Figure 5: Evolution of estimates $\hat{\lambda}(w^*)$ and $\hat{\nu}^{\beta^*}(w^*)$ over training epoch for minima found by SGD and entropy-SGD in feedforward ReLU network for MNIST. We observe that $\hat{\lambda}(w^*)$ rises over training and stabilize to specific values. Both $\hat{\lambda}(w^*)$ and $\hat{\nu}^{\beta^*}(w^*)$ are lower for networks trained with entropy-SGD, throughout training.

in Figure 10 which shows comprehensive results reflecting the effect of γ and chain length T . We see that our observation about SGD and entropy-SGD are relatively robust to these hyperparameters. Interestingly Figure 2 also reveals that the local learning coefficient estimate has remarkably low variance over the randomness of the stochastic optimiser. Finally it is noteworthy that the local learning coefficient estimate of a learned NN model for both stochastic optimisers is, on average, a tiny percentage of the total number of weights in the NN model: $\hat{\lambda}(w^*) \approx 1000$.

It is also informative to examine the local singular fluctuation estimates. Figure 4 show that the functional variance for entropy-SGD is lower, in other words, SGD seems to explore parts of parameter space where the local posterior covers a more diverse range of functions. We see in Figure 5 that both $\hat{\lambda}(w^*)$ and $\hat{\nu}^{\beta^*}(w^*)$ increase with training epoch.

11 Conclusion

We reviewed the two central quantities in Singular Learning Theory, the learning coefficient λ and the singular fluctuation ν . We introduced local versions that are amenable to scalable estimation and of intrinsic interest. In particular, the local learning coefficient quantifies the degree of degeneracy exhibited by a learned neural network. We have seen that degeneracy is more than just counting the number of directions in parameter space where the loss does not change. This is why Hessian-based measures of complexity cannot account for the true nature of degeneracy in singular models. An exciting direction of future research is to employ the local learning coefficient and local singular fluctuation in detecting phase transitions and emergent abilities in deep learning models.

Acknowledgement

SW is the recipient of an Australian Research Council Discovery Early Career Researcher Award (project number DE200101253) funded by the Australian Government. SW is also partially funded by an unrestricted gift from Google. We would like to thank Liam Carroll, Garrett Baker, Quintin Pope, Simon Pepin Lehalleur, Zach Furman, and Jesse Hoogland for discussions and valuable feedback on the manuscript.

References

- Aoyagi, M. and Watanabe, S. (2005). Stochastic complexities of reduced rank regression in Bayesian estimation. *Neural Networks*, 18(7):924–933.
- Aoyagi, M. and Watanabe, S. (2006). Resolution of Singularities and the Generalization Error with Bayesian Estimation for Layered Neural Network. *IEICE Trans*, pages 2112–2124.
- Balasubramanian, V. (1997). Statistical inference, Occam’s razor, and statistical mechanics on the space of probability distributions. *Neural Computation*, 9(2):349–368.
- Banyaga, A. and Hurtubise, D. E. (2004). A proof of the Morse-Bott lemma. *Expo. Math.*, 22(4):365–373.
- Bleistein, N. and Handelsman, R. (1986). *Asymptotic Expansions of Integrals*. Dover Books on Mathematics Series. Dover Publications.
- Chaudhari, P., Choromanska, A., Soatto, S., LeCun, Y., Baldassi, C., Borgs, C., Chayes, J., Sagun, L., and Zecchina, R. (2019). Entropy-SGD: Biasing gradient descent into wide valleys. *Journal of Statistical Mechanics: Theory and Experiment*, 2019(12):124018.
- Chen, D., Chang, W., and Chaudhari, P. (2023). Learning Capacity: A Measure of the Effective Dimensionality of a Model.
- Deng, L. (2012). The MNIST database of handwritten digit images for machine learning research. *IEEE Signal Processing Magazine*, 29(6):141–142.
- Friel, N., McKeone, J. P., Oates, C. J., and Pettitt, A. N. (2017). Investigation of the widely applicable Bayesian information criterion. *Statistics and Computing*, 27:833–844.
- Friel, N. and Pettitt, A. N. (2008). Marginal Likelihood Estimation via Power Posteriors. *Journal of the Royal Statistical Society. Series B (Statistical Methodology)*, 70(3):589–607.
- Hironaka, H. (1964). Resolution of Singularities of an Algebraic Variety Over a Field of Characteristic Zero: I. *Annals of Mathematics*, 79(1):109–203.
- Hoffman, M. D. and Gelman, A. (2014). The No-U-turn sampler: adaptively setting path lengths in hamiltonian monte carlo. *J. Mach. Learn. Res.*, 15(1):1593–1623.
- Imai, T. (2019). Estimating Real Log Canonical Thresholds. *arXiv:1906.01341 [math, stat]*.
- Jiang, Y., Neyshabur, B., Mobahi, H., Krishnan, D., and Bengio, S. (2019). Fantastic Generalization Measures and Where to Find Them. In *International Conference on Learning Representations*.
- LaMont, C. H. and Wiggins, P. A. (2019). Correspondence between thermodynamics and inference. *Physical Review E*, 99(5):052140.
- Le, S. L. S. a. Q. V. (2018). A Bayesian Perspective on Generalization and Stochastic Gradient Descent. In *International Conference on Learning Representations*.
- Liang, T., Poggio, T., Rakhlin, A., and Stokes, J. (2019). Fisher-Rao Metric, Geometry, and Complexity of Neural Networks. In *Proceedings of the Twenty-Second International Conference on Artificial Intelligence and Statistics*, pages 888–896. PMLR.
- Novak, R., Bahri, Y., Abolafia, D. A., Pennington, J., and Sohl-Dickstein, J. (2018). Sensitivity and generalization in neural networks: an empirical study. In *International Conference on Learning Representations*.
- Schwarz, G. (1978). Estimating the Dimension of a Model. *The Annals of Statistics*, 6(2):461–464.
- Watanabe, S. (2007). Almost All Learning Machines are Singular. In *2007 IEEE Symposium on Foundations of Computational Intelligence*, pages 383–388.
- Watanabe, S. (2009). *Algebraic Geometry and Statistical Learning Theory*. Cambridge University Press, USA.
- Watanabe, S. (2010). Equations of states in singular statistical estimation. *Neural Networks*, 23(1):20–34.

- Watanabe, S. (2013). A Widely Applicable Bayesian Information Criterion. *Journal of Machine Learning Research*, 14(Mar):867–897.
- Watanabe, S. (2018). *Mathematical Theory of Bayesian Statistics*. CRC Press, Taylor and Francis group, USA.
- Wei, S., Murfet, D., Gong, M., Li, H., Gell-Redman, J., and Quella, T. (2022). Deep Learning Is Singular, and That’s Good. *IEEE Transactions on Neural Networks and Learning Systems*, pages 1–14.
- Welling, M. and Teh, Y. W. (2011). Bayesian learning via stochastic gradient langevin dynamics. In *Proceedings of the 28th International Conference on Machine Learning*.
- Zhang, C., Bengio, S., Hardt, M., Recht, B., and Vinyals, O. (2017). Understanding deep learning requires rethinking generalization. In *Proceedings of the 5th International Conference on Learning Representations*.
- Zhang, Y., Saxe, A. M., Advani, M. S., and Lee, A. A. (2018). Energy–entropy competition and the effectiveness of stochastic gradient descent in machine learning. *Molecular Physics*, 116(21-22):3214–3223.

A Bayesian Learning

Much of singular learning theory is concerned with Bayesian learning of singular models. The learning coefficient and singular fluctuation make important appearances in these results, which we review in this section.

In contrast to point estimation, Bayesian learning proceeds by *marginalisation*. The full Bayesian learning approach uses the so-called Bayesian posterior predictive distribution,

$$p^\beta(y|x, \mathcal{D}_n) = \int p(y|x, w)p^\beta(w|\mathcal{D}_n) dw.$$

We also consider an alternative Bayesian learning method whereby a single draw from the posterior is used as a point estimate. This is known as Gibbs learning (Watanabe, 2009).

To each of these Bayesian learners, we can associate the generalisation errors

$$\begin{aligned} B_g &:= \text{KL}(q(y|x) \| p^\beta(y|x, \mathcal{D}_n)), \\ G_g &:= \mathbb{E}_w^\beta \text{KL}(q(y|x) \| p(y|x, w)). \end{aligned}$$

The letters B and G stand for Bayesian and Gibbs learning respectively. These generalisation errors have corresponding training errors:

$$\begin{aligned} B_t &:= K_n(q(y|x) \| p^\beta(y|x, \mathcal{D}_n)), \\ G_t &:= \mathbb{E}_w^\beta K_n(q(y|x) \| p(y|x, w)) \end{aligned}$$

where K_n is the empirical KL divergence in (13).

We will use $\mathbb{E}_{\mathcal{D}_n}$ to denote the expectation over the training datasets \mathcal{D}_n . The singular fluctuation ν in (8) characterises the Bayesian and Gibbs generalisation gaps in the following sense. It was established in (Watanabe, 2010) that the (expected) Bayes quartet errors, B_g, B_t, G_g, G_t , are determined by λ and ν :

$$\begin{aligned} \mathbb{E}_{\mathcal{D}_n} B_g &= \frac{\lambda + \nu\beta - \nu}{n\beta} + o(1/n), \\ \mathbb{E}_{\mathcal{D}_n} B_t &= \frac{\lambda - \nu\beta - \nu}{n\beta} + o(1/n), \\ \mathbb{E}_{\mathcal{D}_n} G_g &= \frac{\lambda + \nu\beta}{n\beta} + o(1/n), \\ \mathbb{E}_{\mathcal{D}_n} G_t &= \frac{\lambda - \nu\beta}{n\beta} + o(1/n). \end{aligned}$$

It then follows that

$$\begin{aligned} \mathbb{E}_{\mathcal{D}_n} B_g &= \mathbb{E}_{\mathcal{D}_n} B_t + 2\beta(\mathbb{E}_{\mathcal{D}_n} G_t - \mathbb{E}_{\mathcal{D}_n} B_t) + o(1/n), \\ \mathbb{E}_{\mathcal{D}_n} G_g &= \mathbb{E}_{\mathcal{D}_n} G_t + 2\beta(\mathbb{E}_{\mathcal{D}_n} G_t - \mathbb{E}_{\mathcal{D}_n} B_t) + o(1/n). \end{aligned}$$

Watanabe (2010) shows that the singular fluctuation characterises the gaps $(\mathbb{E}_{\mathcal{D}_n} B_g - \mathbb{E}_{\mathcal{D}_n} B_t)$ and $(\mathbb{E}_{\mathcal{D}_n} G_g - \mathbb{E}_{\mathcal{D}_n} G_t)$ by showing that

$$n\beta(\mathbb{E}_{\mathcal{D}_n} G_t - \mathbb{E}_{\mathcal{D}_n} B_t) \rightarrow \nu^\beta.$$

A.1 Local Bayesian learning

We give analogous results to Appendix A for the local posterior predictive distribution,

$$\mathbb{E}_{w|w^*, \gamma}^\beta [p(y|x, w)].$$

We assume that w^* is a local minimum $L(w)$ and investigate a sufficiently small neighbourhood V of w^* satisfying the assumptions stated in Section 6. We drop the constant term in the generalisation error B_g to arrive at the **test cross-entropy loss** of the local posterior predictive distribution

$$BL_g(w^*, \gamma) := -\mathbb{E}_q \log \left(\mathbb{E}_{w|w^*, \gamma}^\beta p(y|x, w) \right).$$

If w^* is a local minimum of $L(w)$ in a γ -neighbourhood, then we can adapt the results in Appendix A to obtain the expectation of the local Bayes generalisation error

$$\mathbb{E}_{\mathcal{D}_n} BL_g(w^*, \gamma) = L(w^*) + \lambda(w^*)/n + o(1/n). \quad (21)$$

Note that this decomposes into a bias term $L(w^*)$ and a variance term $\lambda(w^*)/n$ which dispels the notion that the local learning coefficient itself determines test error.

Similarly, the test cross-entropy loss corresponding to the local Gibbs learner,

$$GL_g(w^*, \gamma) := -\mathbb{E}_{w|w^*, \gamma}^\beta \mathbb{E}_q \log p(y|x, w)$$

admits the following asymptotic relation:

$$\mathbb{E}_{\mathcal{D}_n} GL_g(w^*, \gamma) = L(w^*) + \frac{\lambda(w^*) + \nu(w^*)}{n} + o(1/n). \quad (22)$$

B MNIST Experiments details

In this experiment, we trained a feedforward ReLU network on the MNIST dataset Deng (2012). The dataset consists of 60000 training samples and 10000 testing samples. The network is designed with 2 hidden layers having sizes [1024, 1024], and it contains a total of 1863690 parameters.

For training, we employed two different optimizers, SGD and entropy-SGD, minimizing cross-entropy loss. Both optimizers are set to have learning rate of 0.01, momentum parameter at 0.9 and batch size of 512. SGD is trained with Nesterov look-ahead gradient estimator. The number of samples L used by entropy-SGD for local free energy estimation is set to 5. The network is trained for 200 epochs. The number of epochs is chosen so that the classification error rate on the training set falls below 10^{-4} .

After each epoch of training, we run local SGLD sampling to compute $\hat{\lambda}(w^*)$ and $\hat{\nu}^{\beta^*}(w^*)$ for w^* set to the network parameter reached at that epoch. The localizing prior scale parameter γ is set to 100.0. The hyperparameters used for SGLD approximate posterior sampling are as follows: ϵ is set to 10^{-5} , the number of steps taken in an SGLD chain is set to 400 and the minibatch size is taken to be the same as the batch size used for both SGD and entropy-SGD training above, i.e. 512. We repeat each SGLD chain 4 times to compute the variance of estimated quantities and also as a diagnostic tool, a proxy for estimation stability. The reported $\hat{\nu}^{\beta^*}(w^*)$ is the average value of the estimates from the 4 independent chains.

The experiments are repeated for 80 RNG seeds.

Figure 6 shows the training and testing error curves over training epochs for both optimizers.

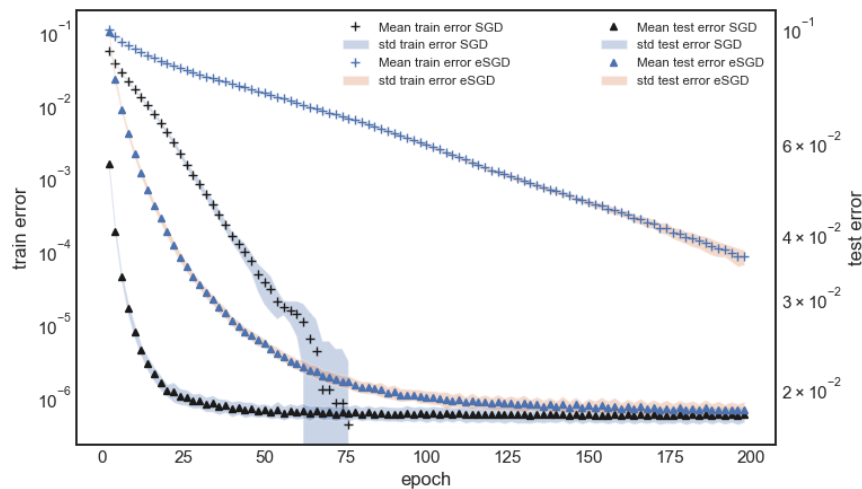


Figure 6: Classification error rate for training (left axis, + marker) and testing (right axis, triangle marker) datasets for both optimizers: SGD in black and entropy-SGD in blue. Note the log-scale for both axis on which zero error cannot be shown. The training cutoff of 200 epoch is chosen so that both optimizers can reach training error $< 10^{-4}$.

C Pseudocode and discussion for estimation algorithms

Full details of the algorithms used for $\hat{\lambda}(w^*)$ and $\hat{\nu}^{\beta^*}(w^*)$ estimation are given in Algorithms 1 and 2 respectively. Code is available at https://github.com/edmundlth/scalable_learning_coefficient_with_sgld/tree/v1.0.

Note that for estimation of $\hat{\lambda}(w^*)$ in MNIST, we use a minibatch estimate $L_m(w)$ of the full training data negative log-likelihood $L_n(w)$. This vastly improves memory and compute efficiency. However, for MNIST $\hat{\nu}^{\beta^*}(w^*)$, current implementation requires accumulation of the log-likelihood $\log p(y_i | x_i, w)$ at every data point (x_i, y_i) in the full dataset \mathcal{D}_n for every SGLD sampled parameter w . While this is not an issue for small datasets like MNIST, alternative more efficient algorithms for calculating variance are required for further scalability.

For experiments involving synthetic data, we set mini-batch size $m = n$, i.e. full-batch.

C.1 Observed issues and possible improvement in future work

Based on observations of SGLD sampling in MNIST and on toy potentials, there are a few ways that SGLD sampling can fail to produce good $\hat{\lambda}(w^*)$ estimates:

- **Large ϵ :** There seems to be a threshold ϵ above which, if the SGLD trajectory encounters a large value of $L_m(w)$, this causes a runaway effect where subsequent $L_m(w)$ and $\nabla_w L_m(w)$ values become larger and eventually exceed machine floating point number upper limits.
- **Negative $\hat{\lambda}(w^*)$:** This happens when w^* fails to be a local minimum or when the SGLD trajectory wanders to a lower potential area causing the numerator in (20) to be negative. This could be alleviated by shorter chain length (risks under-exploration) or larger restoring force γ (risks the issue discussed below).
- **Large γ :** As shown in Figure 9, an overly concentrated localising prior (γ too large) can overwhelm the gradient signal coming from the log-likelihood. This can result in samples that are different from the posterior, destroying SGLD’s sensitivity to the local geometry.

There are various possible future improvements.

- **Incorporate HMC / NUTS:** Currently, all SGLD steps are taken to be approximate posterior samples. To produce better coverage of the local posterior, we could incorporate ideas from Hamiltonian Monte Carlo samplers with added Gaussian noise where samples are generated with better exploration of the local potential landscape. Furthermore, automatic tuning of hyperparameters in the NUTS variant of the sampler could resolve the issues with the current sampler’s sensitivity to hyperparameters.
- **Accept-reject steps:** Having an accept-reject step could help produce more reliable samples at the cost of longer runtime. Furthermore, this could resolve the issue mentioned above regarding samples drawn with extremely low likelihood.
- **Multi-temperature posterior samples:** The paper which introduced the WBIC Watanabe (2013) proposed the use of sampling from tempered posteriors at multiple inverse temperatures, e.g. β_1, β_2 , and estimating the local coefficient by

$$\hat{\lambda} = \frac{\mathbb{E}_w^{\beta_1}[nL_n(w)] - \mathbb{E}_w^{\beta_2}[nL_n(w)]}{\frac{1}{\beta_1} - \frac{1}{\beta_2}}.$$

This requires running multiple sampling chains and thus increasing the compute budget. With careful handling of potential numerical overflow issue, one can potentially use the formula below, pointed out in the same paper, to convert samples from one chain to be samples from another temperature:

$$\mathbb{E}_w^{\beta_2}[f(w)] = \frac{\mathbb{E}_w^{\beta_1}[f(w)e^{(\beta_2-\beta_1)nL_n(w)}]}{\mathbb{E}_w^{\beta_1}[e^{(\beta_2-\beta_1)nL_n(w)}}}.$$

- **Better diagnostic tools:** We can incorporate better diagnostic tools in addition to checking standard deviation of the estimated quantities across multiple independent SGLD chains. For example, tracking acceptance rate at accept-reject steps and tracking the norms of $\nabla_w L_m(w)$ could help with detecting failures in SGLD exploration.

Algorithm 1 computing $\hat{\lambda}(w^*)$

Input: initialisation point w^* , scale γ , SGLD ϵ , SGLD chain length T , SGLD minibatch m , training data $\mathcal{D}_n = \{(x_i, y_i)\}_{i=1, \dots, n}$, and averaged log-likelihood function for $w \in \mathbb{R}^d$ and arbitrary batch D of data:

$$\log L(D, w) = \frac{1}{|D|} \sum_{(x_i, y_i) \in D} \log p(y_i | x_i, w)$$

Output: $\hat{\lambda}(w^*)$

```

1:  $w \leftarrow w^*$  ▷ Initialise at the given parameter
2: arrayLogL  $\leftarrow []$ 
3: for  $t = 1 \dots T$  do
4:    $B \leftarrow$  random minibatch of size  $m$ 
5:   append  $\log L(B, w)$  to arrayLogL
6:    $\eta \sim N(0, \epsilon)$  ▷  $d$ -dimensional Gaussian, variance  $\epsilon$ 
7:    $\Delta w \leftarrow \frac{\epsilon}{2} [\gamma(w^* - w) + n\beta^* \nabla_w \log L(B, w)] + \eta$ 
8:    $w \leftarrow w + \Delta w$ 
9: end for
10:  $\text{WBIC} \leftarrow -n \cdot \text{Mean}(\text{arrayLogL})$ 
11:  $nL_n(w^*) \leftarrow -n \cdot \log L(\mathcal{D}_n, w^*)$ 
12:  $\hat{\lambda}(w^*) \leftarrow \frac{\text{WBIC} - nL_n(w^*)}{\log n}$ 
13: return  $\hat{\lambda}(w^*)$ 

```

Algorithm 2 computing $\hat{\nu}^{\beta^*}(w^*)$

Input: Same as Algorithm 1

Output: $\hat{\nu}^{\beta^*}(w^*)$

```

1:  $w \leftarrow w^*$  ▷ Initialise at given parameter
2:  $M \leftarrow 0$ 
3: arrayLogL  $\leftarrow \text{zeros}(n)$  ▷ array of zeros of size  $n$ 
4: sqArrayLogL  $\leftarrow \text{zeros}(n)$  ▷ array of zeros of size  $n$ 
5: for  $t = 1 \dots T$  do
6:    $M \leftarrow M + 1$ 
7:   for  $i = 1 \dots n$  do
8:      $x \leftarrow \log L((x_i, y_i), w)$ 
9:     arrayLogL $_i \leftarrow$  arrayLogL $_i + x$ 
10:    sqArrayLogL $_i \leftarrow$  sqArrayLogL $_i + x^2$ 
11:   end for
12:    $B \leftarrow$  random minibatch of size  $m$ 
13:   append  $\log L(B, w)$  to arrayLogL
14:    $\eta \sim N(0, \epsilon)$  ▷  $d$ -dimensional Gaussian noise
15:    $\Delta w \leftarrow \frac{\epsilon}{2} [\gamma(w^* - w) + n\beta^* \nabla_w \log L(B, w)] + \eta$ 
16:    $w \leftarrow w + \Delta w$ 
17: end for
18:  $\text{Variance}_i \leftarrow \frac{1}{M} \sum_{i=1}^M \text{sqArrayLogL}_i - \text{arrayLogL}_i^2$ 
19:  $\hat{\nu}^{\beta^*}(w^*) \leftarrow \frac{\beta^*}{2} \sum_{i=1}^n \text{Variance}_i$ 
20: return  $\hat{\nu}^{\beta^*}(w^*)$ 

```

D More normal crossing posteriors

In Section 10.1 we used models in normal crossing form to test the sensitivity of SGLD samples to local geometry. In this appendix we extend this analysis to a more significant test by incorporating varying priors. This requires some slight deviations from the theoretical setting of the main text which we now explain.

Note that in our definition of the local learning coefficient $\lambda(w^*)$ we introduced a local posterior (19) with a prior contribution $\varphi_\gamma(w - w^*)$ that ignores the prior $\bar{\varphi}$ of the local triplet from Section 6. The justification for this is that, provided $\bar{\varphi} > 0$ at w^* which is generally true in our applications, the prior contributes only $O(1)$ terms to the

monomial	prior	λ	MCMC				SGLD ($\epsilon = 0.0001$)				SGLD ($\epsilon = 0.0005$)			
			$\hat{\lambda}$		$\hat{\nu}^{\beta^*}$		$\hat{\lambda}$		$\hat{\nu}^{\beta^*}$		$\hat{\lambda}$		$\hat{\nu}^{\beta^*}$	
			mean	std	mean	std	mean	std	mean	std	mean	std	mean	std
$w_1^1 w_2^3$	$w_1^0 w_2^0$	0.17	0.12	0.04	0.17	0.03	0.10	0.09	0.11	0.07	0.11	0.07	0.14	0.05
$w_1^1 w_2^3$	$w_1^1 w_2^0$	0.17	0.17	0.01	0.17	0.01	0.14	0.10	0.14	0.07	0.16	0.05	0.18	0.04
$w_1^1 w_2^2$	$w_1^0 w_2^0$	0.25	0.19	0.11	0.32	0.16	0.10	0.10	0.16	0.12	0.14	0.12	0.23	0.09
$w_1^2 w_2^3$	$w_1^0 w_2^4$	0.25	0.17	0.13	0.17	0.05	0.30	0.20	0.12	0.04	0.27	0.07	0.14	0.03
$w_1^3 w_2^1$	$w_1^1 w_2^1$	0.33	0.34	0.04	0.30	0.04	0.29	0.16	0.22	0.16	0.28	0.07	0.29	0.09
$w_1^0 w_2^1$	$w_1^0 w_2^0$	0.50	0.41	0.12	0.50	0.04	0.42	0.13	0.51	0.03	0.45	0.11	0.54	0.04
$w_1^1 w_2^0$	$w_1^0 w_2^0$	0.50	0.43	0.12	0.49	0.03	0.45	0.14	0.50	0.05	0.47	0.13	0.53	0.05
$w_1^1 w_2^1$	$w_1^0 w_2^0$	0.50	0.33	0.15	0.44	0.04	0.29	0.18	0.40	0.12	0.32	0.14	0.42	0.06
$w_1^3 w_2^1$	$w_1^3 w_2^3$	0.67	0.58	0.29	0.45	0.28	0.67	0.22	0.19	0.08	0.63	0.23	0.29	0.14
$w_1^2 w_2^1$	$w_1^2 w_2^3$	0.75	0.79	0.16	0.26	0.18	0.71	0.23	0.25	0.13	0.66	0.17	0.27	0.11
$w_1^4 w_2^1$	$w_1^6 w_2^3$	0.88	0.76	0.46	0.44	0.30	0.77	0.33	0.22	0.06	0.81	0.30	0.23	0.06
$w_1^1 w_2^1$	$w_1^1 w_2^1$	1.00	0.80	0.15	0.83	0.15	0.75	0.25	0.75	0.25	0.92	0.22	1.09	0.32

Table 2: Estimates $\hat{\lambda}(w^*)$ and $\hat{\nu}^{\beta^*}(w^*)$ (with standard deviation) for the integrals discussed in Appendix D, using posterior samples from MCMC or SGLD. The hyperparameters of SGLD are set to batch size $m = n$, chain length $T = 10,000$ and ϵ set to values indicate in the column headers. The estimated local learning coefficients correlate well with their true values. See Figure 7 for accompanying visualisation. Note that this table is a superset of table 1a, where the uniform prior is represented by the case where the prior monomial is $w_1^0 w_2^0$.

asymptotic (18). However, in order to test the ability of SGLD sampling to reproduce known theoretical values of λ it is also interesting to consider cases where the prior vanishes at w^* to some order. This is relevant because of the normal form discussed in Section 2.

We fix $(k_1, k_2), (h_1, h_2) \in \mathbb{N}^2$ and test the ability of SGLD sampling to discover the $\log n$ coefficient in the asymptotic expansion of

$$-\log \int \exp(-nCw_1^{2k_1} w_2^{2k_2}) |w_1^{h_1} w_2^{h_2}| dw_1 dw_2 \quad (23)$$

for some positive constant C whose actual value is inconsequential. The theoretical value of the coefficient is given by $\lambda = \min\{\frac{h_1+1}{2k_1}, \frac{h_2+1}{2k_2}\}$.

To this end, we consider the parameter space $[-5, 5]^2$ equipped with a uniform prior, effectively setting $b = 1$ in (3). Let the input x be sampled from a standard Gaussian and output y be modelled $y = \rho(w_1, w_2)x + N(0, \sigma^2)$ where $\rho(w_1, w_2) = w_1^{k_1} w_2^{k_2}$ is a monomial and $\sigma^2 = 1/4$ is the variance of the observation noise. A synthetic training data set of size $n = 1000$ is generated where the true parameter is chosen to be $w^* = (0, 0)$. This is constructed so that $K(w) = Cw_1^{2k_1} w_2^{2k_2}$ for some positive constant C and $W_0 = \{(w_1, w_2) \in \mathbb{R}^2 : w_1 w_2 = 0\}$. We choose a prior in normal crossing form, $\varphi(w_1, w_2) \propto |w_1^{h_1} w_2^{h_2}|$ supported on $[-5, 5]^2$. The stylised posterior is therefore

$$p(w | \mathcal{D}_\infty) \propto \exp(-nCw_1^{2k_1} w_2^{2k_2}) |w_1^{h_1} w_2^{h_2}|.$$

The only change we need to make to methodology of Section 10.1 is to adjust the SGLD update from Section 7.1 to

$$\begin{aligned} \Delta w_t = & \frac{\epsilon}{2} \left(\beta^* \sum_{i=1}^n \nabla \log p(y_i | x_i, w_t) \right. \\ & \left. + \nabla \log |w_t^h| + \gamma(w^* - w_t) \right) + N(0, \epsilon) \end{aligned}$$

where if $w_t = (w_{t,1}, w_{t,2})$ then $|w_t^h| = |w_{t,1}^{h_1} w_{t,2}^{h_2}|$. All other experimental details are as in Section 10.1. The trend of $\hat{\lambda}$ vs λ values are shown in Figure 7. The full data can be found in Table 2.

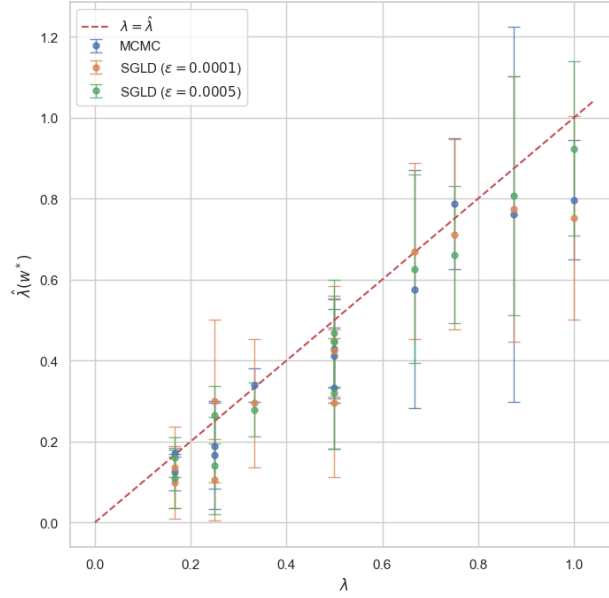


Figure 7: As a companion visualisation to Table 2, we plot $\hat{\lambda}(w^*)$ against $\lambda(w^*)$ for the MCMC and SGLD with two choices of ϵ .

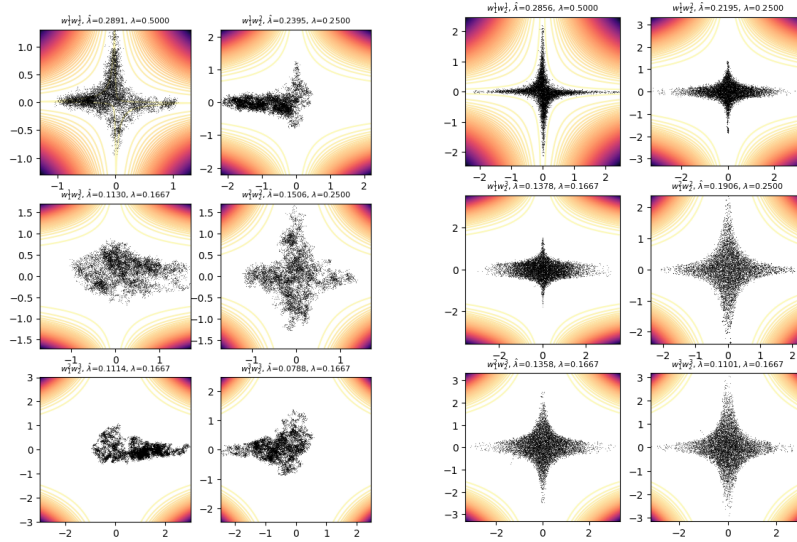


Figure 8: Additional figure for Section 10.1. Sampling paths for stylised posterior with $K(w_1, w_2) = w_1^{2k_1} w_2^{2k_2}$ for various combination of (k_1, k_2) . Left set: SGLD, right set: MCMC

E Additional figures

Figures 8, 9, and 10 are additional figures for the experiments in Section 10.

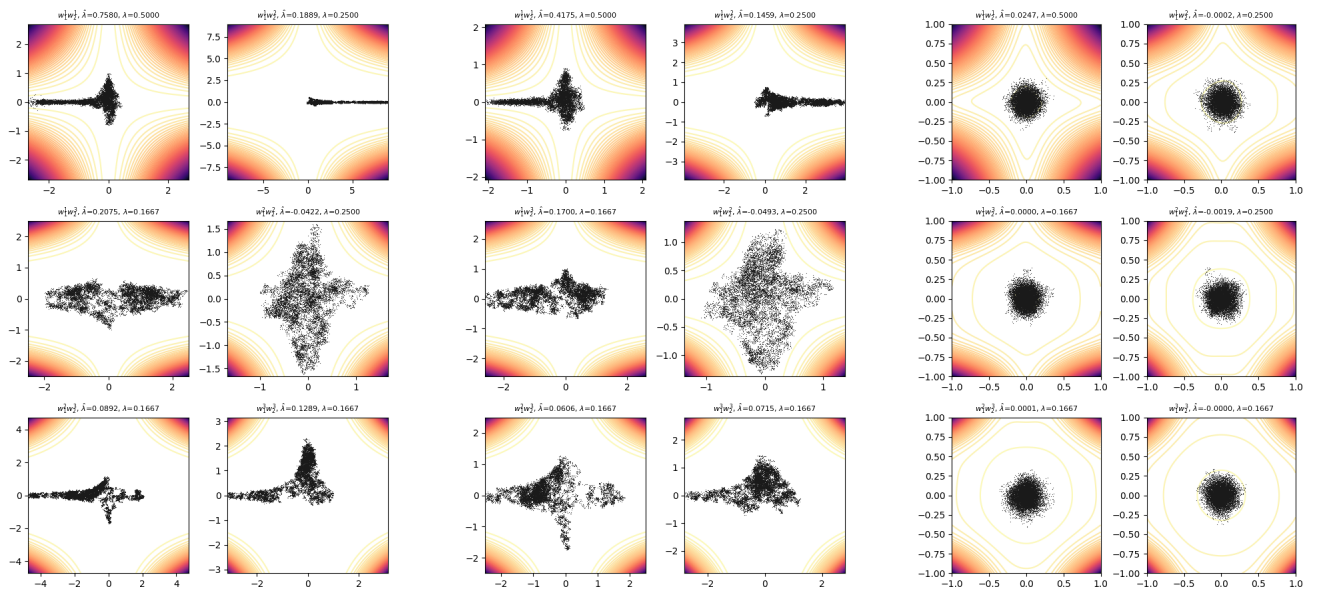


Figure 9: Additional figure for Section 10.1. These sample paths illustrates the role of the scale parameter γ for SGLD with the same set up in Figure 8. For overly small γ such as the those on the left figure (note the scale on axes) could result in trajectories that wander far from w^* . This could cause issue when the trajectory visits neighbourhood with different loss and degeneracy. On the other hand, a large γ such as those on the right figure would cause the localising prior to dominate signals from the likelihood. Left: $\gamma = 0.0001$. Middle: $\gamma = 1$. Right: $\gamma = 10000$.

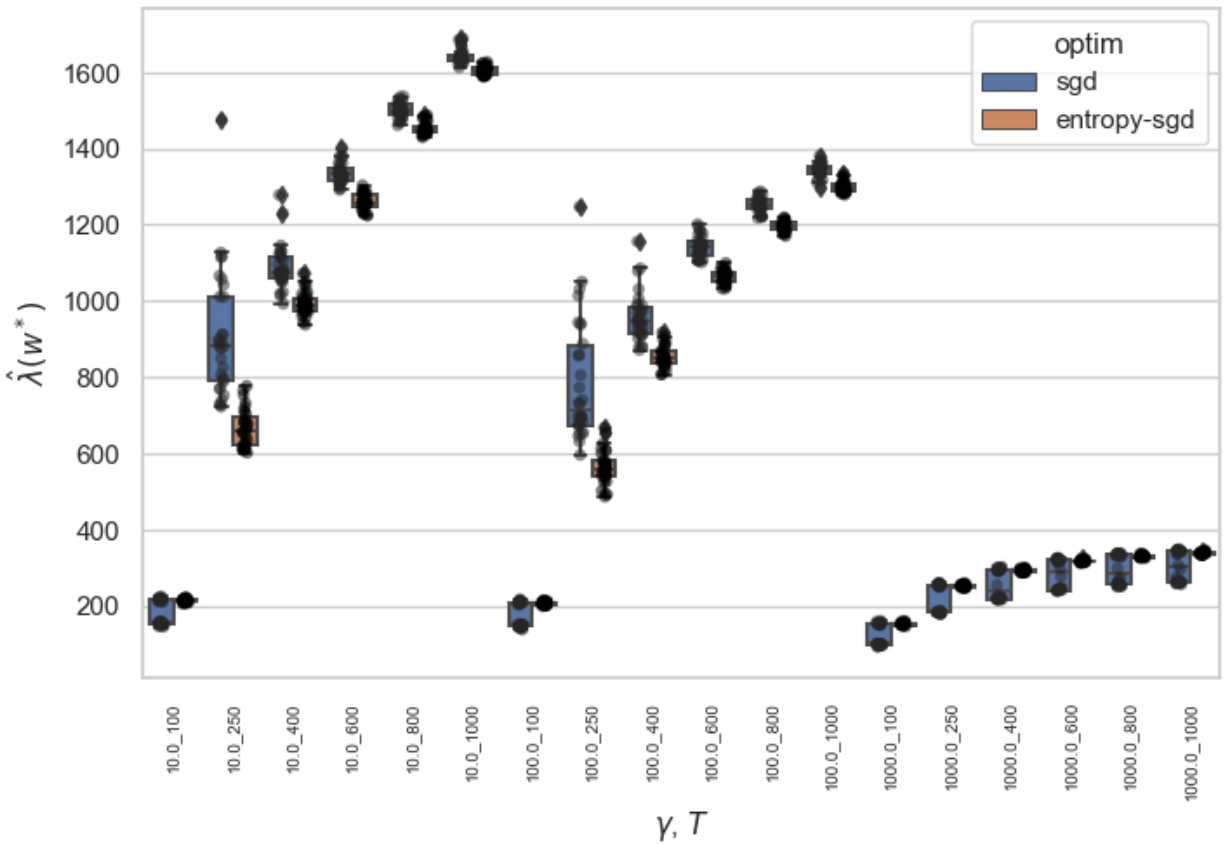


Figure 10: Additional figure for Section 10.3. These boxplots show the estimates $\hat{\lambda}(w^*)$ with different SGLD hyperparameters: $\gamma = 10, 100, 1000$ and SGLD chain length $T = 100, 250, 400, 600, 800, 1000$. The hyperparameters should be chosen so that the SGLD trajectory sufficiently explores the neighbourhood around w^* without being dominated by the localising Gaussian prior controlled by γ . The chain length T should ideally be as long as possible and the figure show that a chain length of 100 appears to be insufficient. With increasing chain length, $\hat{\lambda}(w^*)$ trends upwards and possibly asymptotes towards certain finite value while the variance becomes smaller. The choice of chain length is thus a balance between compute budget and estimation variance. For γ , observe that overly constraining prior (large γ) seems to induce similar issues with small chain length.